

---

# DeformRS: Certifying Input Deformations with Randomized Smoothing

---

Motasem Alfarra\*  
KAUST

Adel Bibi\*  
University of Oxford

Naeemullah Khan  
University of Oxford

Philip H. S. Torr  
University of Oxford

Bernard Ghanem  
KAUST

## Abstract

Deep neural networks are vulnerable to input deformations in the form of vector fields of pixel displacements and to other parameterized geometric deformations *e.g.* translations, rotations, etc. Current input deformation certification methods either (i) do not scale to deep networks on large input datasets, or (ii) can only certify a specific class of deformations, *e.g.* only rotations. We reformulate certification in randomized smoothing setting for both general vector field and parameterized deformations and propose DEFORMRS-VF and DEFORMRS-PAR, respectively. Our new formulation scales to large networks on large input datasets. For instance, DEFORMRS-PAR certifies rich deformations, covering translations, rotations, scaling, affine deformations, and other visually aligned deformations such as ones parameterized by Discrete-Cosine-Transform basis. Extensive experiments on MNIST, CIFAR10 and ImageNet show that DEFORMRS-PAR outperforms existing state-of-the-art in certified accuracy, *e.g.* improved certified accuracy of 6% against perturbed rotations in the set  $[-10^\circ, 10^\circ]$  on ImageNet. Our code is available at [github.com/MotasemAlfarra/DeformRS](https://github.com/MotasemAlfarra/DeformRS).

## 1 Introduction

Deep Neural Networks (DNNs) are susceptible to small additive input perturbations, *i.e.* a DNN that correctly classifies  $x$  can be fooled into misclassifying  $(x + \delta)$ , even when  $\delta$  is so small that  $x$  and  $(x + \delta)$  are imperceptibly different [1, 2]. Even worse, DNNs were shown to be vulnerable to input deformations [3] such as input rotations and scaling, where such deformations, unlike additive perturbations, can exist due to a slight change in the physical world. This raises a critical concern especially since DNNs are now deployed in safety critical applications, *e.g.* self-driving cars. To address the nuisance of sensitivity to input deformations, one would ideally seek to train DNNs that are *certifiably* free from such adversaries. While there has been impressive progress towards this goal, *i.e.* certifying input deformations, prior art suffers from the limitation of only being able to certify an individual set of deformations, *e.g.* only rotations or only translations etc., or a small composition set of them [4–6]. Only recently has a certification approach been developed for the richer class of smooth vector fields (general displacement of pixels) [7]. However, all previous approaches require solving a mixed-integer or linear program, thus limiting their applicability to small DNNs on small datasets. On the contrary, the only certification methods that scale to larger networks on large datasets (*e.g.* ImageNet) are based on randomized smoothing [8]. However, such approaches [9, 10], similar to many others, are limited to individual deformations, *e.g.* only translations, or to deformations that ought to be *resolvable*, thus limiting the overall class of certifiable deformations.

---

\*Joint first authorship. Correspondance to: [motasem.alfarra@kaust.edu.sa](mailto:motasem.alfarra@kaust.edu.sa) and [adel.bibi@eng.ox.ac.uk](mailto:adel.bibi@eng.ox.ac.uk).

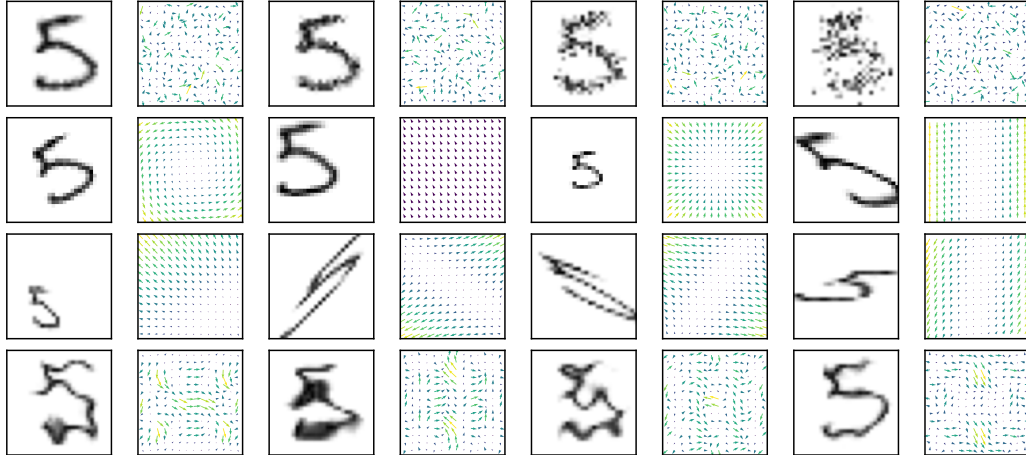


Figure 1: **Examples of deformations.** We show examples of image deformations accompanied with their respective vector fields. First row: Gaussian random deformations. Second row: rotation, translation, scaling, and shearing. Third row: affine deformations. Last row: DCT deformations.

In this paper, we address the aforementioned limitations in current prior art in one framework through randomized smoothing. Our approach, dubbed DEFORMRS, is general, and it allows for the certification of vector field *and* parameterized deformations. For the class of parameterized deformations, DEFORMRS certifies general affine deformations that cover translation, rotations, scaling, shearing, etc., and any composition of them. Moreover, we show that if the parameterized deformation is represented by the low frequency components of the Discrete Cosine Transform (DCT), DEFORMRS allows for the certification of a set of visually aligned and plausible deformations. Figure 1 presents several examples of the class of deformations DEFORMRS certifies at scale. Our contributions can be summarized as follows. **(i) DEFORMRS-VF.** We extend the formulation of randomized smoothing from pixel intensities to vector field deformations and derive a certification radius  $R$  for the deformation vector field. That is to say, DEFORMRS-VF resists all deformations having a vector field with a norm that is smaller than  $R$ . **(ii) DEFORMRS-PAR.** We specialize our analysis for parametrizable deformations and propose DEFORMRS-PAR, which grants certification to popular deformations, *e.g.* translation, rotation, scaling, and any composition subset of them, in addition to the general affine class of deformations. We also specialize DEFORMRS-PAR for the set of deformations parameterized by the low-frequency components of DCT, thus certifying a richer class of visually aligned deformations that were not explored in earlier works. **(iii)** We demonstrate the effectiveness of our proposed approach by conducting extensive experiments on MNIST [11], CIFAR10 [12], and ImageNet [13]. DEFORMRS-VF is capable of providing networks that are certifiably robust against general input deformations. Moreover, DEFORMRS-PAR improves the state-of-the-art certified accuracy against rotation and scaling deformation by (1.25%, 1.9%) on MNIST, (4%, 31%) on CIFAR10, and (6%, 11%) on ImageNet, respectively.

## 2 Related Work

**Certifying Additive Input Perturbations.** Due to the vulnerability of DNNs to adversarial attacks [1, 14], a stream of work was developed to build models that are certifiable against  $\ell_p$  bounded additive adversaries. This includes methods based on Satisfiability Modulo Theory solvers [15–17], interval bound propagation [18], and semi-definite programming [19], among many others [15, 20]. However, this class of approaches is generally computationally expensive for certifying deeper networks on large dimensional inputs [21] let alone for using them as part of a training routine towards training better certifiable networks [22]. Recently, randomized smoothing [23, 8] demonstrated to be an effective and scalable approach for probabilistic certification of additive perturbations. In a nutshell, given a classifier  $f$ , randomized smoothing grants a certification for the classifier  $g$  that outputs the most probable class of  $f$  when the input is subjected to noise sampled from a distribution  $\mathcal{D}$ . Followed by various improvements through incorporating adversarial training [24], regularization

[25], smoothing distribution optimization [26] among many others, randomized smoothing showed to achieve state-of-the-art performance in constructing highly accurate and certifiable networks at the scale of ImageNet. Following the favorable properties of randomized smoothing, we leverage it for our input deformation certification.

**Certifying Image Deformations.** In addition to additive input perturbations, DNNs were shown to be susceptible to input deformations. For instance, it was shown that DNNs can be fooled into mispredicting inputs undergoing small imperceptible vector field deformations (pixel displacements) [3]. This was followed by several works that aim to provide empirical evaluation of robustness against such deformations, *e.g.* input translations and rotations, including attacks and defenses [27–29]. Unlike certification of additive input perturbations, certifying input deformations only recently started gaining attention. For instance, one of the earliest work performs an abstract interval bound propagation for certification [4], which was later followed by a tighter linear program formulation [5], which certifies geometric transformations such as translation and rotation. Recently, several popular geometric transformations as well as other transformations, such as intensity contrast, were formulated as a piece-wise nonlinear layer [6], thus allowing for exact certification based on a tighter formulation of classical  $\ell_p$  certification solvers commonly used for additive perturbations. Moreover, recent work [7] exploited interval bound propagation to certify general vector fields of image deformations. However, all previous methods either inherently suffer from scalability limitations due to the underlying solvers, or that they cannot certify a composition of transformations jointly. Alleviating the scalability constraints, randomized smoothing was deployed to certify image transformations that are invariant to interpolation [30]; however, the proposed formulation was restricted to individual transformations like rotation and translation. This was followed by the work of [10], where networks were verified against individual resolvable transformations by estimating their Lipschitz upper bound. Due to the scalability properties randomized smoothing methods enjoy, we extend prior art to allow for scalable certification of general vector field deformations.

### 3 Certifying Deformations with Randomized Smoothing

**Background.** Randomized smoothing constructs a provably robust classifier  $g : \mathbb{R}^n \rightarrow \mathcal{P}(\mathcal{Y})$  from any classifier  $f : \mathbb{R}^n \rightarrow \mathcal{P}(\mathcal{Y})$ , where  $\mathcal{P}(\mathcal{Y})$  is a probability simplex over the set of labels  $\mathcal{Y}$ . Formally and following [25], one can express the output of  $g$  for some distribution  $\mathcal{D}$  as:

$$g(x) = \mathbb{E}_{\epsilon \sim \mathcal{D}} [f(x + \epsilon)].$$

Suppose that  $g$  assigns the class  $c_A$  for an input  $x$ , we define:

$$p_A = \mathbb{E}_{\epsilon \sim \mathcal{D}} [f^{c_A}(x + \epsilon)] \quad \text{and} \quad p_B = \max_{i \neq c_A} \mathbb{E}_{\epsilon \sim \mathcal{D}} [f^i(x + \epsilon)],$$

where  $f^i(x)$  is the  $i^{\text{th}}$  element of  $f(x)$ . Then, for Gaussian smoothing, *i.e.*  $\mathcal{D} = \mathcal{N}(0, \sigma^2 I)$ ,  $g$  outputs a fixed prediction, *i.e.*  $g(x) = g(x + \delta)$ , for any perturbation  $\delta$  satisfying  $\|\delta\|_2 \leq \frac{\sigma}{2} (\Phi^{-1}(p_A) - \Phi^{-1}(p_B))$  [25]. Here,  $\Phi^{-1}$  is the inverse CDF of the standard Gaussian. Moreover, for uniform smoothing, *i.e.*  $\mathcal{D} = \mathcal{U}[-\lambda, \lambda]$ , then  $g(x) = g(x + \delta)$  for any perturbation  $\delta$  satisfying  $\|\delta\|_1 \leq \lambda(p_A - p_B)$  [31]. While there has been tremendous progress in robustifying networks against  $\ell_p$  additive attacks, there has been far less progress towards robustness against non-additive perturbations (*e.g.* illumination changes, shadowing, input deformations, etc.). In this work, we focus on the rich class of spatial deformations, *i.e.* perturbations to the pixel coordinates, which cover as a special case translation, rotation, zooming in and out, sheering, etc. Figure 1 visualizes examples of deformations certifiable within our framework.

#### 3.1 DEFORMRS-VF: Certifying Vector Fields

**Deformations.** Let the discrete grid  $\Omega^{\mathbb{Z}} \subset \mathbb{Z}^2$ , where  $\mathbb{Z}$  is the set of integers, represent the domain of images  $I : \Omega^{\mathbb{Z}} \rightarrow [0, 1]^c$ , where  $c$  is the number of channels in the image. Then, a domain deformation is defined as  $T : \Omega^{\mathbb{Z}} \rightarrow \mathbb{R}^2$ , such that for a pixel coordinate  $p \in \Omega^{\mathbb{Z}}$ , we can write  $T(p) = p + v(p)$ , where  $v : \Omega^{\mathbb{Z}} \rightarrow \mathbb{R}^2$  represents the vector field. Since the deformation  $T$  maps pixel coordinates to  $\mathbb{R}^2$ , one needs to define an associated interpolation function for a deformed image  $x \in [0, 1]^n$ , where  $n = c \times |\Omega^{\mathbb{Z}}|$ , as  $I_T : [0, 1]^n \times \mathbb{R}^{2|\Omega^{\mathbb{Z}}|} \rightarrow [0, 1]^n$ . As such, when  $T(p) = p \ \forall p \in \Omega^{\mathbb{Z}}$ , then we have  $I_T(x, T(p)) = x$ . For ease of notation, we use  $p$  to denote the complete set of the discrete grid  $\Omega^{\mathbb{Z}}$ . In line with the randomized smoothing framework, we extend the definition of smoothed classifiers to domain deformation smoothed classifiers.

**Definition 1.** Given a classifier  $f : \mathbb{R}^n \rightarrow \mathcal{P}(\mathcal{Y})$  and an interpolation function  $I_T : [0, 1]^n \times \mathbb{R}^{2|\Omega^{\mathbb{Z}}|} \rightarrow [0, 1]^n$ , we define a deformation smoothed classifier as:

$$\hat{g}(x, p) = \mathbb{E}_{\epsilon \sim \mathcal{D}} [f(I_T(x, p + \epsilon))].$$

Note that contrary to  $g$ , which smooths the predictions of  $f$  under additive pixel perturbations,  $\hat{g}$  smooths predictions of  $f$  under pixel coordinate deformations. Similar in spirit to earlier results on randomized smooth for additive perturbations [8, 25], we can show that  $\hat{g}$  is certifiable as per the following Theorem. We leave all proofs to the **Appendix**.

**Theorem 1.** Suppose that  $\hat{g}$  assigns the class  $c_A$  for an input  $x$ , i.e.  $c_A = \arg \max_c \hat{g}^c(x, p)$  with:

$$p_A = \hat{g}^{c_A}(x, p) \quad \text{and} \quad p_B = \max_{i \neq c_A} \hat{g}^i(x, p)$$

then  $\arg \max_c \hat{g}^c(x, p + \psi) = c_A$  for vector field perturbations satisfying:

$$\begin{aligned} \|\psi\|_1 &\leq \lambda(p_A - p_B) && \text{for } \mathcal{D} = \mathcal{U}[-\lambda, \lambda], \\ \|\psi\|_2 &\leq \frac{\sigma}{2} (\Phi^{-1}(p_A) - \Phi^{-1}(p_B)) && \text{for } \mathcal{D} = \mathcal{N}(0, \sigma^2 I), \end{aligned} \quad (1)$$

Theorem 1 states that as long as the  $\ell_1$  and  $\ell_2$  norms of the deformation characterized by the vector field  $\psi$  are sufficiently small, then  $\hat{g}$  enjoys a constant prediction. Note that the  $\ell_1$  and  $\ell_2$  certificates are agnostic to the structure of the deformation vector field  $\psi$ . That is to say,  $\hat{g}$  resists all domain deformations, e.g. translation, rotation, scaling, etc., as long as (1) is satisfied. This also includes patch level deformations, i.e. when  $\psi$  is an all zero vector field except for a set of indices representing a patch (e.g. a rotation of a patch in the image).

### 3.2 DEFORMRS-PAR: Certifying Parametrizable Deformations

Note that the dimensionality of the deformation vector field  $\psi$  is twice (two dimensions of the image) the number of pixel coordinates, i.e.  $2|\Omega^{\mathbb{Z}}|$ , where  $|\Omega^{\mathbb{Z}}| = 32 \times 32$  in CIFAR10. As such, the set of deformation vector fields  $\psi$  of this large dimensionality satisfying the conditions in (1) might be limited to a set of imperceptible deformations, i.e.  $x$  and  $I_T(x, p + \psi)$  are indistinguishable.<sup>2</sup> However, many popular deformations are parameterized by a much smaller set of parameters. In general, consider the deformation  $T_\phi(p) = p + v_\phi(p)$ , where the dimension of  $\phi$  is much lower than  $v_\phi(p)$ , where  $v_\phi$  is an element wise function. For example, when the vector field  $v_\phi$  characterizes a translation or a rotation, the parameterization  $\phi$  is of dimensions 2 and 1, respectively. In that regard, we show that a close relative to Theorem 1 also holds for perturbations in the parameters characterizing deformations. We start by defining a parametric deformation smoothed classifier.

**Definition 2.** Given a classifier  $f : \mathbb{R}^n \rightarrow \mathcal{P}(\mathcal{Y})$  and an interpolation function  $I_T : [0, 1]^n \times \mathbb{R}^{2|\Omega^{\mathbb{Z}}|} \rightarrow [0, 1]^n$ , we define a parametric deformation smoothed classifier as follows:

$$\tilde{g}_\phi(x, p) = \mathbb{E}_{\epsilon \sim \mathcal{D}} [f(I_T(x, p + v_{\phi+\epsilon}(p)))].$$

Unlike Definition 1,  $\tilde{g}_\phi$  smooths the prediction of  $f$  under a specific class of deformations by perturbing the parameterization  $\phi$ . Next, we analyze the certifiable robustness of  $\tilde{g}_\phi$ .

**Corollary 1.** Suppose that  $\tilde{g}$  assigns the class  $c_A$  for an input  $x$ , i.e.  $c_A = \arg \max_c \tilde{g}_\phi^c(x, p)$  with:

$$p_A = \tilde{g}_\phi^{c_A}(x, p) \quad \text{and} \quad p_B = \max_{i \neq c_A} \tilde{g}_\phi^i(x, p),$$

then  $\arg \max_c \tilde{g}_\phi^c(x, p + \xi) = c_A$  for all parametric domain perturbations satisfying:

$$\begin{aligned} \|\xi\|_1 &\leq \lambda(p_A - p_B) && \text{for } \mathcal{D} = \mathcal{U}[-\lambda, \lambda], \\ \|\xi\|_2 &\leq \frac{\sigma}{2} (\Phi^{-1}(p_A) - \Phi^{-1}(p_B)) && \text{for } \mathcal{D} = \mathcal{N}(0, \sigma^2 I). \end{aligned} \quad (2)$$

Corollary 1 specializes the result of Theorem 1 to the family of parametric deformations. It states that as long as the norm of the perturbations to the deformation parameters is sufficiently small as per (2),  $\tilde{g}_\phi$  enjoys a constant prediction. Next, we show the parametrization of several popular deformations. Let the pixel grid  $\Omega^{\mathbb{Z}}$  be the grid of an image of size  $N \times M$ , where  $p_{n,m} = (n, m) \in \Omega^{\mathbb{Z}}$  is a pixel location and  $v_\phi(p_{n,m}) = (u_{n,m}, v_{n,m})$  represents the vector field at  $p_{n,m}$ .

<sup>2</sup>Certifying imperceptible deformations is important in its own right, since adversaries can take this form [3].

**Translation.** Image translation is only parameterized by two parameters  $\phi = \{t_u, t_v\}$ , namely  $v_\phi(p_{n,m}) = (t_u, t_v) \forall p \forall n, m$  as per Definition 2 and Corollary 1.

**Rotation.** 2D rotation is only parameterized by the rotation angle  $\phi = \{\theta\}$ , where  $u_{n,m} = n(\cos(\theta) - 1) - m\sin(\theta)$  and  $v_{n,m} = n\sin(\theta) + m(\cos(\theta) - 1)$  as per Definition 2 and Corollary 1.

**Scaling.** Similar to rotation, scaling is parametrized with one parameter; the scaling factor  $\phi = \{\alpha\}$ , where  $u_{n,m} = (\alpha - 1)n$  and  $v_{n,m} = (\alpha - 1)m \forall n, m$ . That is to say, the vector field has the form  $v_\alpha(p) = ((\alpha - 1)n, (\alpha - 1)m) \forall p$  as per Definition 2 and Corollary 1.

**Affine.** Our formulation for the certification of the parametric family of deformations is general and covers all affine vector fields as special cases. In particular, affine vector fields are parameterized by 6 parameters, namely  $\phi = \{a, b, c, d, e, f\}$ , where  $u_{n,m} = an + bm + e$  and  $v_{n,m} = cn + dm + f$ . Note that this class naturally covers composite deformations, such as scaling and translation jointly.

**Beyond Affine: DCT-Basis.** To address deformations beyond affine vector fields, we also consider certifying a class of deformations represented by the Discrete Cosine Transform (DCT) basis. In particular, we consider the low-frequency component truncated DCT of the vector field  $u_{n,m}$  and  $v_{n,m}$  with a window size of  $k \times k$  (as opposed to the complete size of  $N \times M$ ), where the set is characterized by  $|\phi| = 2k^2$  parameters. We present further details on this in the **Appendix**.

## 4 Experiments

We validate the certified performance of DEFORMRS against both vector field and parameterizable deformations following Theorem 1 and Corollary 1, respectively. The goal of this section is to show that (i) DEFORMRS-PAR improves certified accuracy against individual deformations that are parameterizable (*e.g.* rotation, translation, and scaling), as compared to prior art [6, 10, 5, 32]. (ii) DEFORMRS-PAR can certify the general class of affine deformations allowing for the certification of a composition of deformations, *e.g.* rotation and sheering jointly. (iii) DEFORMRS-PAR can certify deformations that are parameterized by truncated DCT coefficients, a more general class of deformations that can represent visually aligned deformations. (iv) Following Theorem 1, DEFORMRS-VF certifies general vector field deformations that are generally imperceptible.

**Setup.** We follow standard practices from prior art [8, 10, 32] to conduct experiments on MNIST [11], CIFAR10 [12] and ImageNet [13] datasets. For experiments on MNIST and CIFAR10, we certify ResNet18 [33] trained for 90 epochs with a learning rate of 0.1, momentum of 0.9, weight decay of  $10^{-4}$ , and learning rate decay at epochs 30 and 60 by a factor of 0.1. For ImageNet experiments, we certify a fine-tuned pretrained ResNet50 for 30 epochs using SGD with a learning rate of  $10^{-3}$  that decays at every 10 epochs by a factor of 0.1. All networks are trained with data augmentation sampled from the respective deformations that are being certified, so as to attain a highly accurate base classifier  $f$  under such deformations. Following randomized smoothing methods [8, 24–26] and using publicly available code [8], all our results are certified with 100 Monte Carlo samples for the selection of the top prediction  $c_A$  and 100,000 samples for the estimation of a lower bound to the prediction probability  $p_A$  with a failure probability of 0.001. Throughout all experiments, we choose  $I_T$  to be a bi-linear interpolation function. We compare against both mixed integer and linear program based certification methods [5, 6], as well as randomized smoothing based approaches [34, 10]. Note that, since image dimensions vary across datasets (square images of sizes 28, 32, 224 for MNIST, CIFAR10 and ImageNet, respectively), we normalize all image dimensions to  $[-1, 1] \times [-1, 1]$ .

**Evaluation metrics.** Following the certification literature [8, 25, 10], we use certified accuracy to compare networks. The certified accuracy at a radius  $R$  is the percentage of the test set that is both correctly classified and has a certification radius of at least  $R$ . Note that  $R$  is computed following Corollary 1 for DEFORMRS-PAR and following Theorem 1 for DEFORMRS-VF.

We also report the Average Certified Radius (ACR) [25]:  $\frac{1}{|\mathcal{S}_{test}|} \sum_{(x,y) \in \mathcal{S}_{test}} R(f_\theta, x) \mathbb{1}\{g_\theta(x) = y\}$ , where  $\mathbb{1}$  is an indicator function and  $R$  is the certification radius computed as per Theorem 1 and Corollary 1.



Table 1: **Certifying individual deformations on MNIST and CIFAR10.** We compare the certified accuracy of DEFORMRS-PAR against (R)otation, (S)caling and (T)ranslation with that of prior art. We define  $\|\psi\|_2 = (t_u^2 + t_v^2)^{1/2}$  for translation. (a) and (d): Certified accuracy at  $T(\|\psi\|_2 \leq 2)$  and  $T(\|\psi\|_2 \leq 2.41)$ , respectively; we adopt these settings from [5, 9] for fair comparison. (b) and (c): Certified accuracy at  $R(6.79^\circ)$  and  $R(38.24^\circ)$ , respectively; we adopt these settings from [9]. Note that DEFORMRS-PAR achieves a higher certified accuracy than (a, b, d) at a higher radius. Best certified accuracies are highlighted in bold.

Certification	MNIST			CIFAR-10		
	R(30°)	S(20%)	T( $\ \psi\ _2 \leq 5$ )	R(10°)	S(20%)	T( $\ \psi\ _2 \leq 5$ )
[5, 6]	87.80 [5]	-	77.00 <sup>(a)</sup> [5]	21.80 [6], 87.80[5]	-	-
[9]	72.75 <sup>(c)</sup>	-	95.00 <sup>(d)</sup>	42.00 <sup>(b)</sup>	-	-
[10]	95.60	96.80	96.80	63.80	58.40	84.80
DEFORMRS-PAR	<b>96.85, 96.10<sup>(c)</sup></b>	<b>98.70</b>	<b>99.20</b>	<b>91.82</b>	<b>90.30</b>	<b>88.80</b>

Table 2: **Certifying individual deformations on ImageNet.** We compare the certified accuracy of DEFORMRS-PAR against (R)otation, (S)caling and (T)ranslation with prior art. (e): Certified accuracy at  $R(1.86^\circ)$ ; we adopt this setting from [9]. Best certified accuracies are highlighted in bold.

Certification	ImageNet		
	R(10°)	S (15%)	T( $\ \psi\ _2 \leq 5$ )
[9]	17.25 <sup>(e)</sup>	-	-
[10]	33.00	31.00	<b>63.30</b>
DEFORMRS-PAR	<b>39.00</b>	<b>42.80</b>	48.20

#### 4.1 DEFORMRS-PAR against Individual Parameterizable Deformations<sup>3</sup>

**Rotation.** Rotation deformations are parameterized with a bounded scalar representing the rotation angle  $\theta \in [-\pi, \pi]$ . Therefore, we use the Uniform smoothing variant of Corollary 1 resulting in a certification of the form  $|\theta| \leq \lambda(p_A - p_B)$ . We train several networks with  $\lambda \in \{\pi/10, 2\pi/10, \dots, \pi\}$ , where each trained network is certified with the corresponding  $\lambda$  used in training.

We compare the rotation certified accuracy of DEFORMRS-PAR against that of prior work [5, 6, 9, 10] on MNIST and CIFAR10 in Table 1 and on ImageNet in Table 2. Following the common practice in randomized smoothing literature [24, 25], Tables 1 and 2 report the best certified accuracies for DEFORMRS-PAR cross-validated over  $\lambda$ .

In particular, and as shown in Table 1, DEFORMRS-PAR outperforms its best competitor by 1.25% and 4% on MNIST and CIFAR-10 at rotation radii of  $30^\circ$  (i.e.  $R(30^\circ)$ ) and  $10^\circ$  (i.e.  $R(10^\circ)$ ), respectively. Interestingly, on CIFAR10, the certified accuracy of DEFORMRS-PAR at radius  $10^\circ$  is even better than the accuracy of [9] reported at the smaller angle radius of  $6.79^\circ$ . The improvement is consistent on ImageNet, where DEFORMRS-PAR outperforms the randomized smoothing based approach of [10] by 6%, as reported in Table 2. We believe that DEFORMRS-PAR outperforms mixed-integer and linear program rotation certification methods due to their high computational cost that results in prohibitive explicit training for improved certification [5–7]. Moreover, DEFORMRS-PAR does not require the resolvability assumption common in randomized smoothing approaches [10]. We plot in the first column of Figure 2 the certified accuracy of DEFORMRS-PAR over a subset  $\lambda$  used for training and certification. We leave the rest of the ablations of  $\lambda$  to the **Appendix**. We observe that the certified accuracies of DEFORMRS-PAR at the radii reported in the previous tables are indeed insensitive to the choice of  $\lambda$ . Moreover, we note that DEFORMRS-PAR attains a certified accuracy of at least 80% on both MNIST and CIFAR10 at a radius of  $100^\circ$ . In addition, when  $\lambda = 90^\circ$  on MNIST, DEFORMRS-PAR attains an ACR of  $85^\circ$ , i.e. the average certified rotation is  $85^\circ$ .

**Scaling.** Scaling deformations are parameterized by  $\alpha \geq 0$ . Note that a scaling  $\alpha$  can either be a zoom-out ( $\alpha > 1$ ) or a zoom-in ( $0 < \alpha < 1$ ). For ease, we consider the bounded scaling factor  $\alpha - 1$  instead such that  $|\alpha - 1| < 0.7$ . Thus, an appropriate smoothing distribution in Corollary 1 is uniform with  $\lambda \in \{0.1, 0.2, \dots, 0.7\}$  granting a certificate of the form  $|\alpha - 1| \leq \lambda(p_A - p_B)$ . We report the certified accuracy at the scale factor of 20% (i.e.  $0.8 \leq \alpha \leq 1.20$ ) in Table 1 for MNIST

<sup>3</sup>Compared to additive pixel certification, certifying image deformations is a less studied research area, so no standard benchmarks or evaluation protocols exist yet. This is why we define several superscripts in Tables 1 and 2, as different comparative methods have reported certified accuracies at different radii.

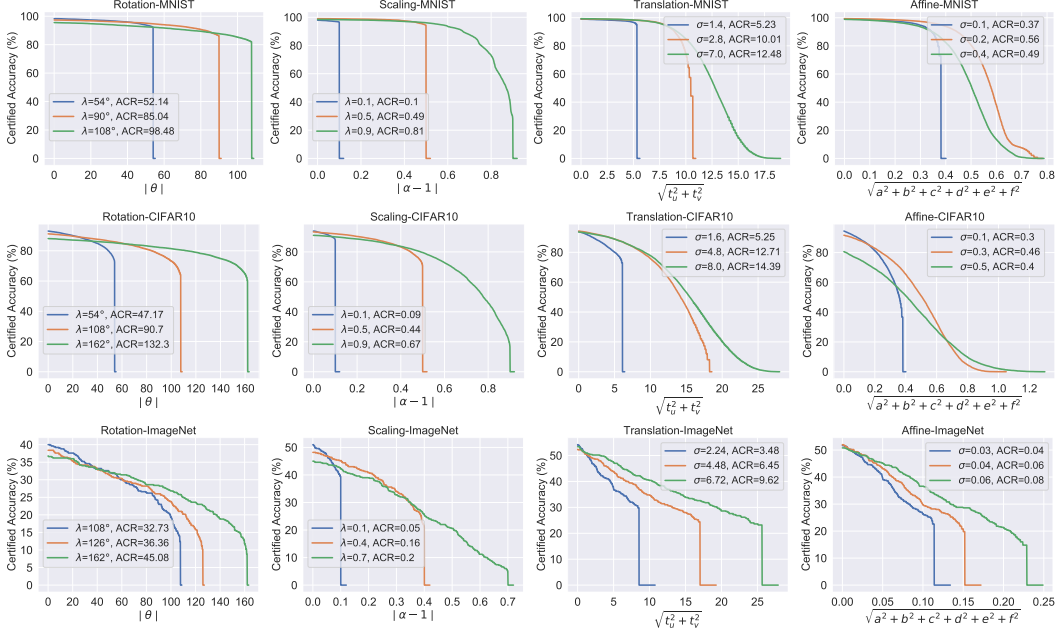


Figure 2: **Certified performance of DEFORMRS-PAR.** We show the effect of varying the smoothing parameters ( $\lambda$ ,  $\sigma$ ) on the certified accuracy of DEFORMRS-PAR against rotation, scaling, translation, and affine deformations.

and CIFAR10, and at a scale factor of 15% (*i.e.*  $0.85 \leq \alpha \leq 1.15$ ) for ImageNet in Table 2. The best certified accuracy cross validated over  $\lambda$  for DEFORMRS-PAR outperforms its best competitor [10] by 1.9% on MNIST, 31.9% on CIFAR10, and 11.8% on ImageNet. Moreover, we plot the certified accuracy in the second column of Figure 2 showing the insensitivity of DEFORMRS-PAR to  $\lambda$ . Moreover, DEFORMRS-PAR enjoys a certified accuracy of at least (90%, 80%, 40%) at the larger scaling factors of (0.5, 0.4, 0.2) on MNIST, CIFAR10 and ImageNet, respectively.

**Translation.** Contrary to rotation and scaling, translation deformations are parameterized by two parameters ( $t_u, t_v$ ) that can generally be of any value. So for this experiment, we employ two dimensional Gaussian smoothing as per Corollary 1, where  $\sigma \in \{0.1, 0.2, \dots, 0.5\}$  for MNIST and CIFAR10, and  $\sigma \in \{0.02, 0.03, \dots, 0.06\}$  for ImageNet. In this case, the granted certificate is of the form  $(t_u^2 + t_v^2)^{1/2} \leq \sigma/2(\Phi^{-1}(p_A) - \Phi^{-1}(p_B))$ . We compare against [5, 6, 10] and report the certified accuracy at a certification radius of at most 5 pixels<sup>4</sup>. As observed from Table 1, DEFORMRS-PAR outperforms its best competitor by 2% and 4% on MNIST and CIFAR10, respectively. However, we observe that DEFORMRS-PAR underperforms on ImageNet attaining 48.2% certified accuracy compared to 63.3% by [10] as reported in Table 2. We believe that DEFORMRS-PAR performs worse on ImageNet due to the suboptimal training of the base classifier  $f$  on ImageNet. This is evident in the third column of Figure 2, which plots the certified accuracy over a range of different radii for several smoothing  $\sigma$ . Note that the certified accuracy of DEFORMRS-PAR is  $\sim 52\%$  at radius 0 over all  $\sigma$ . That is to say, the *accuracy* of DEFORMRS-PAR is already worse than the *certified accuracy* at radius 5 reported by [10]. However, the certified accuracy of DEFORMRS-PAR for MNIST and CIFAR10 at radii of 7 and 8 pixels are at least 90% and 80% on MNIST and CIFAR10, respectively.

## 4.2 DEFORMRS-PAR against Affine Deformations

Attaining high certified accuracy for individual deformations, as discussed earlier, requires the training of networks for these particular deformations. In this subsection, we leverage Corollary 1 to certify the more general affine deformation. We train a *single* DEFORMRS-PAR network against affine deformations, where we certify this network against several specializations of the affine certificate. As

<sup>4</sup>Since the image dimensions in our setting are normalized to  $[-1, 1]$ , we unnormalize the radius results to pixels in the original image for comparison and ease of interpretation in Figure 2.



Figure 3: **Examples of certified affine deformations.** We sample affine parameters satisfying the affine certification inequality of DEFORMRS-PAR and apply them to MNIST and ImageNet images.

discussed earlier, the affine deformation is parameterized by 6 parameters, and the vector field is given as  $u_{n,m} = an + bm + e$  and  $v_{n,m} = cn + dm + f$ . Since generally, there are no restrictions on the values of the affine parameters, we use Gaussian smoothing in Corollary 1 to sample  $\{a, b, c, d, e, f\}$  with  $\sigma \in \{0.1, 0.2, \dots, 0.5\}$  for MNIST and CIFAR10 and  $\sigma \in \{0.02, 0.03, \dots, 0.06\}$  on ImageNet. The certificate is therefore in the form  $\sqrt{a^2 + b^2 + c^2 + d^2 + e^2 + f^2} \leq \sigma/2(\Phi^{-1}(p_A) - \Phi^{-1}(p_B))$ . We plot our results in the last column of Figure 2, which summarizes the certified accuracy of DEFORMRS-PAR on all three datasets. For instance, as per Figure 2, the certified accuracy of DEFORMRS-PAR at affine radius of 0.3 on MNIST is 90%. This is equivalent, under specialization to a translation (*i.e.*  $a = b = c = d = 0$ ), to a certified accuracy of 90% for all translations of radius  $0.15 \times 24 = 4.2$  pixels (after unnormalization to image dimensions).

**Composition of deformations.** We specialize the certification to a composition of several deformations and compare against the only work (to the best of our knowledge) on certifying deformation compositions [5]. Following [5], we first consider the composition of shearing with a factor of  $s$  followed by rotation with angle  $\theta$ . In this case, the vector field is given as follows:

$$\begin{pmatrix} u_{n,m} \\ v_{n,m} \end{pmatrix} = \underbrace{\begin{pmatrix} \cos(\theta) & -\sin(\theta) \\ \sin(\theta) & \cos(\theta) \end{pmatrix}}_{\text{rotation}} \underbrace{\begin{pmatrix} 1 & s \\ 0 & 1 \end{pmatrix}}_{\text{shear}} \begin{pmatrix} n \\ m \end{pmatrix} - \begin{pmatrix} n \\ m \end{pmatrix}.$$

We leave the details of the above Equation to the **Appendix**. Note that this composition can be formulated as an affine deformation with  $a = \cos(\theta) - 1$ ,  $b = s \cos(\theta) - \sin(\theta)$ ,  $c = \sin(\theta)$ ,  $d = s \sin(\theta) + \cos(\theta) - 1$ , and  $e = f = 0$ . Therefore, Corollary 1 grants the following certificate  $\sqrt{s^2 - 2s \sin(\theta) - 4 \cos(\theta) + 4} \leq \sigma/2(\Phi^{-1}(p_A) - \Phi^{-1}(p_B))$ . We compare against [5], which achieves a certified accuracy of 54.2% on CIFAR10 under the setting  $|\theta| \leq 2^\circ$  and  $0 \leq s \leq 2\%$ . To compute the certified accuracy of DEFORMRS-PAR, note that the left hand side achieves its maximum of 0.0651 at  $\theta^* = -2^\circ$  and  $s^* = 0.02$ ; thus, the certified accuracy of DEFORMRS-PAR is the percentage of the test set classified correctly with a radius of at least 0.0651. DEFORMRS-PAR achieves a certified accuracy of 91.28% on CIFAR10 and 43.6% on ImageNet as per the last column in Figure 2, thus outperforming [5] by 37%. Note that, our affine certification allows for the seamless certification of all considered deformations in the literature. This surpasses any need to specialize a certificate for every deformation family of an affine nature. In fact, with a single network trained with DEFORMRS-PAR against affine deformations, we achieve non-trivial certified accuracies against several specialized deformations. Moreover, we consider certifying the same DEFORMRS-PAR network under the composition of a rotation of angle  $\theta$ , scaling by factor  $\alpha$ , and a translation of parameters  $(t_u, t_v)$  with a vector field given as follows:

$$\begin{pmatrix} u_{n,m} \\ v_{n,m} \end{pmatrix} = \underbrace{\begin{pmatrix} \alpha & 0 \\ 0 & \alpha \end{pmatrix}}_{\text{scale}} \underbrace{\begin{pmatrix} \cos(\theta) & -\sin(\theta) \\ \sin(\theta) & \cos(\theta) \end{pmatrix}}_{\text{rotation}} \begin{pmatrix} n \\ m \end{pmatrix} + \underbrace{\begin{pmatrix} t_u \\ t_v \end{pmatrix}}_{\text{translation}} - \begin{pmatrix} n \\ m \end{pmatrix}$$

Note that under such a setting, we have  $a = \alpha \cos(\theta) - 1$ ,  $b = -\alpha \sin(\theta)$ ,  $c = \alpha \sin(\theta)$ ,  $d = \alpha \cos(\theta) - 1$ ,  $e = t_u$ , and  $f = t_v$ . Therefore, this grants the following certificate  $\sqrt{2 + 2\alpha^2 - 4\alpha \cos(\theta) + t_u^2 + t_v^2} \leq \sigma/2(\Phi^{-1}(p_A) - \Phi^{-1}(p_B))$ . We consider certifying DEFORMRS-PAR under the composite deformation of  $|\theta| \leq 10^\circ$ ,  $0.8 \leq \alpha \leq 1.2$ , and  $t_u^2 + t_v^2 \leq 0.1$ , where 0.1 corresponds to a radius of 4 and 5 pixels of translation for images in MNIST and CIFAR10, respectively. To that end, we observe that the left hand side of the certificate attains a maximum of 0.503, at which DEFORMRS-PAR enjoys a certified accuracy of 79.78% on MNIST and 50.41% on CIFAR10 as per the last column in Figure 2. To the best of our knowledge, this work is the first to consider such a composite deformation. In Figure 3, we sample several certifiable affine deformations



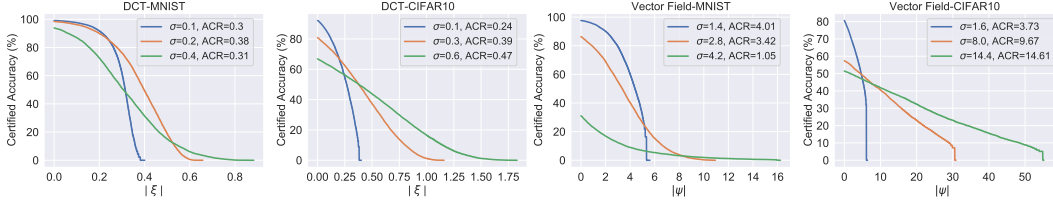


Figure 4: **Performance of DEFORMRS-VF and DEFORMRS-PAR.** We plot the certified accuracy curves of DEFORMRS-PAR against truncated DCT deformations (left) and DEFORMRS-VF against general vector field deformations (right).



Figure 5: **Examples of certified truncated DCT.** We sample truncated DCT coefficients that satisfy the certification inequality of DEFORMRS-PAR and apply them to MNIST and CIFAR10 images.

that satisfy the certificate inequality and apply them to MNIST and ImageNet images. We can observe the richness of the certifiable affine maps in both datasets.

### 4.3 DEFORMRS-PAR against Truncated DCT Deformations

While the class of affine deformations covers several deformations of interest along with their compositions, we go beyond affine deformations in this section to cover parameterized truncated DCT deformations. In particular, we are interested in the class of vector field deformations generated by taking the inverse DCT transform of a truncated window of size  $k \times k \times 2$ . We observe that this class of deformations can generate visually aligned deformations, which are generally not affine, as shown in Figure 1. Note that since the  $k \times k \times 2$  DCT coefficients can take any values, we use Gaussian smoothing with  $\sigma \in \{0.1, 0.2, \dots, 0.5\}$  as per Corollary 1. This grants a certificate of the form  $\|\xi\|_2 \leq \sigma/2(\Phi^{-1}(p_A) - \Phi^{-1}(p_B))$ , where  $\xi$  is the perturbation in the DCT coefficients. For simplicity, we set  $k = 2$  for all the experiments in this section. As summarized in Figure 4, DEFORMRS-PAR certifies perturbations in the DCT coefficients with a certified accuracy of 90% and 80% at radius 0.2 on MNIST and CIFAR10, respectively. Unlike the case of individual deformations or their compositions, it is generally difficult to interpret the certified class of DCT deformations. So, we visualise several samples from the certified region of DCT coefficients in Figure 5. We observe several interesting certified deformations that are visually aligned with semantic perturbations resembling different hand written digits in MNIST or ripples in CIFAR10.

### 4.4 DEFORMRS-VF against General Vector Field Deformations

We leverage Theorem 1 to certify against a general vector field deformation  $\psi$ . Note that such vector fields are in general of size  $N \times M \times 2$  and can take any values. Thus, Gaussian smoothing is an appropriate choice, where we set  $\sigma \in \{0.1, 0.2, \dots, 0.5\}$ . Similar to translations and for ease of interpretation, we plot in the second row of Figure 4 the certified accuracy of DEFORMRS-VF for an unnormalized vector field. We observe that DEFORMRS-VF achieves a certified accuracy of 90% and 60% at a radius of 2 pixels on MNIST and CIFAR10, respectively. Note that while vector field deformations can specialize to all previously considered deformations as special cases (*e.g.* rotations), they enjoy very large dimensionality ( $\psi$  is of size  $2NM$ ) and the resulting certification radius is often very small. This only grants certifications to imperceptible deformations. For instance, consider the vector field generated from a parameterized translation such that  $(t_u^2 + t_v^2)^{1/2} \leq 2$ . The corresponding vector field will have an energy of at most  $\sqrt{2MN}$ . That is to say, to certify vector field deformations representing translations of 2 pixels in  $\ell_2$ , the certification radius of the vector field should be at least  $\sqrt{2MN}$ , which is significantly larger than the radius 2 with the earlier reported accuracy. This is a classical trade-off between the generality of the deformation family (certifying vector fields as opposed to the lower dimensional parameterization) and the imperceptibility of the

certifiable deformation – a classical curse of dimensionality that exists in randomized smoothing in general [35]. Although the certifiable deformations here are not very meaningful (do not represent well-known geometric deformations), this setting is still of interest, since imperceptible deformations can act as adversaries [3]. We refer interested readers to the **Appendix** for qualitative visualizations of certifiable vector field deformations under DEFORMRS-VF.

## 5 Conclusion

We revisit the certification of deformations, pixel coordinate displacements, and following recent advances in randomized smoothing, we propose DEFORMRS-VF DEFORMRS-PAR certifying general vector fields and any parameterizable set of deformations. The parameterizable set of deformations is rich covering individual deformations, *e.g.* rotations, and several compositions, affine deformations and the deformations characterized by truncated DCT coefficients. We conduct several experiments comparing against prior art. Despite its simplicity, our approach is effective to defend against all types of input deformations from the simple individual and parametrizable ones to their most general vector field counterparts. We leave to future work the rigorous analysis of projecting DCT components into individual deformations, *i.e.* finding the maximum certifiable angle given a certificate on the DCT coefficients.

**Acknowledgments.** This work was partially supported by the King Abdullah University of Science and Technology (KAUST) Office of Sponsored Research.

## References

- [1] Christian Szegedy, Wojciech Zaremba, Ilya Sutskever, Joan Bruna, Dumitru Erhan, Ian Goodfellow, and Rob Fergus. Intriguing properties of neural networks, 2014. 1, 2
- [2] Ian J. Goodfellow, Jonathon Shlens, and Christian Szegedy. Explaining and harnessing adversarial examples, 2015. 1
- [3] Rima Alaifari, Giovanni S Alberti, and Tandri Gauksson. Adef: an iterative algorithm to construct adversarial deformations. *International Conference on Learning Representations (ICLR)*, 2019. 1, 3, 4, 10
- [4] Gagandeep Singh, Timon Gehr, Markus Püschel, and Martin Vechev. An abstract domain for certifying neural networks. *Proceedings of the ACM on Programming Languages*, 2019. 1, 3
- [5] Mislav Balunovic, Maximilian Baader, Gagandeep Singh, Timon Gehr, and Martin Vechev. Certifying geometric robustness of neural networks. In *Advances in Neural Information Processing Systems*. Curran Associates, Inc., 2019. 3, 5, 6, 7, 8
- [6] Jeet Mohapatra, Tsui-Wei Weng, Pin-Yu Chen, Sijia Liu, and Luca Daniel. Towards verifying robustness of neural networks against a family of semantic perturbations. In *Proceedings of the IEEE/CVF Conference on Computer Vision and Pattern Recognition (CVPR)*, 2020. 1, 3, 5, 6, 7
- [7] Anian Ruoss, Maximilian Baader, Mislav Balunović, and Martin Vechev. Efficient certification of spatial robustness, 2021. 1, 3, 6
- [8] Jeremy M Cohen, Elan Rosenfeld, and J Zico Kolter. Certified adversarial robustness via randomized smoothing. *International Conference on Machine Learning (ICML)*, 2019. 1, 2, 4, 5, 16
- [9] Marc Fischer, Maximilian Baader, and Martin Vechev. Certified defense to image transformations via randomized smoothing. *Advances in Neural Information Processing Systems (NeurIPS)*, 2020. 1, 6
- [10] Linyi Li, Maurice Weber, Xiaojun Xu, Luka Rimanic, Tao Xie, Ce Zhang, and Bo Li. Provable robust learning based on transformation-specific smoothing, 2020. 1, 3, 5, 6, 7
- [11] Yann LeCun. The mnist database of handwritten digits. <http://yann.lecun.com/exdb/mnist/>, 1998. 2, 5

- [12] Alex Krizhevsky and Geoffrey Hinton. Learning multiple layers of features from tiny images. Technical report, Citeseer, 2009. 2, 5
- [13] Olga Russakovsky, Jia Deng, Hao Su, Jonathan Krause, Sanjeev Satheesh, Sean Ma, Zhiheng Huang, Andrej Karpathy, Aditya Khosla, Michael Bernstein, et al. Imagenet large scale visual recognition challenge. *International Journal of Computer Vision (IJCV)*, 2015. 2, 5
- [14] Ian J. Goodfellow, Jonathon Shlens, and Christian Szegedy. Explaining and harnessing adversarial examples, 2015. 2
- [15] Ruediger Ehlers. Formal verification of piece-wise linear feed-forward neural networks. In *International Symposium on Automated Technology for Verification and Analysis*, 2017. 2
- [16] Guy Katz, Clark Barrett, David L Dill, Kyle Julian, and Mykel J Kochenderfer. Reluplex: An efficient smt solver for verifying deep neural networks. In *International Conference on Computer Aided Verification*, pages 97–117. Springer, 2017.
- [17] Rudy Bunel, Ilker Turkaslan, Philip HS Torr, Pushmeet Kohli, and M Pawan Kumar. A unified view of piecewise linear neural network verification. *arXiv preprint arXiv:1711.00455*, 2017. 2
- [18] Sven Gowal, Krishnamurthy Dvijotham, Robert Stanforth, Rudy Bunel, Chongli Qin, Jonathan Uesato, Relja Arandjelovic, Timothy A. Mann, and Pushmeet Kohli. On the effectiveness of interval bound propagation for training verifiably robust models. *CoRR*, abs/1810.12715, 2018. 2
- [19] Aditi Raghunathan, Jacob Steinhardt, and Percy S Liang. Semidefinite relaxations for certifying robustness to adversarial examples. In S. Bengio, H. Wallach, H. Larochelle, K. Grauman, N. Cesa-Bianchi, and R. Garnett, editors, *Advances in Neural Information Processing Systems*. Curran Associates, Inc., 2018. 2
- [20] Xiaowei Huang, Marta Kwiatkowska, Sen Wang, and Min Wu. Safety verification of deep neural networks. In *International Conference on Computer Aided Verification*, 2017. 2
- [21] Vincent Tjeng, Kai Xiao, and Russ Tedrake. Evaluating robustness of neural networks with mixed integer programming. *International Conference on Learning Representations (ICLR)*, 2019. 2
- [22] Tsui-Wei Weng, Huan Zhang, Hongge Chen, Zhao Song, Cho-Jui Hsieh, Duane Boning, Inderjit S Dhillon, and Luca Daniel. Towards fast computation of certified robustness for relu networks. *International Conference on Machine Learning (ICML)*, 2018. 2
- [23] Mathias Lecuyer, Vaggelis Atlidakis, Roxana Geambasu, Daniel Hsu, and Suman Jana. Certified robustness to adversarial examples with differential privacy. In *IEEE Symposium on Security and Privacy (SP)*. IEEE, 2019. 2
- [24] Hadi Salman, Jerry Li, Ilya Razenshteyn, Pengchuan Zhang, Huan Zhang, Sebastien Bubeck, and Greg Yang. Provably robust deep learning via adversarially trained smoothed classifiers. In *Advances in Neural Information Processing Systems (NeurIPS)*, 2019. 2, 5, 6, 14
- [25] Runtian Zhai, Chen Dan, Di He, Huan Zhang, Boqing Gong, Pradeep Ravikumar, Cho-Jui Hsieh, and Liwei Wang. Macer: Attack-free and scalable robust training via maximizing certified radius. *International Conference on Learning Representations (ICLR)*, 2020. 3, 4, 5, 6
- [26] Motasem Alfarra, Adel Bibi, Philip H. S. Torr, and Bernard Ghanem. Data dependent randomized smoothing, 2020. 3, 5
- [27] Can Kanbak, Seyed-Mohsen Moosavi-Dezfooli, and Pascal Frossard. Geometric robustness of deep networks: analysis and improvement, 2017. 3
- [28] Eric Wong, Frank R. Schmidt, and J. Zico Kolter. Wasserstein adversarial examples via projected sinkhorn iterations, 2020.
- [29] Logan Engstrom, Brandon Tran, Dimitris Tsipras, Ludwig Schmidt, and Aleksander Madry. Exploring the landscape of spatial robustness. In *International Conference on Machine Learning*, pages 1802–1811. PMLR, 2019. 3

- [30] Alexander Levine and Soheil Feizi. Wasserstein smoothing: Certified robustness against wasserstein adversarial attacks, 2019. 3
- [31] Greg Yang, Tony Duan, J. Edward Hu, Hadi Salman, Ilya Razenshteyn, and Jerry Li. Randomized smoothing of all shapes and sizes, 2020. 3
- [32] Marc Fischer, Maximilian Baader, and Martin Vechev. Statistical verification of general perturbations by gaussian smoothing, 2020. 5
- [33] Kaiming He, Xiangyu Zhang, Shaoqing Ren, and Jian Sun. Deep residual learning for image recognition. In *Proceedings of the IEEE conference on computer vision and pattern recognition*, 2016. 5
- [34] Marc Fischer, Maximilian Baader, and Martin Vechev. Certified defense to image transformations via randomized smoothing. In H. Larochelle, M. Ranzato, R. Hadsell, M. F. Balcan, and H. Lin, editors, *Advances in Neural Information Processing Systems*, volume 33, pages 8404–8417. Curran Associates, Inc., 2020. 5
- [35] Aounon Kumar, Alexander Levine, Tom Goldstein, and Soheil Feizi. Curse of dimensionality on randomized smoothing for certifiable robustness. In Hal Daumé III and Aarti Singh, editors, *Proceedings of the 37th International Conference on Machine Learning*, volume 119 of *Proceedings of Machine Learning Research*, pages 5458–5467. PMLR, 13–18 Jul 2020. 10
- [36] Adam Paszke, Sam Gross, Francisco Massa, Adam Lerer, James Bradbury, Gregory Chanan, Trevor Killeen, Zeming Lin, Natalia Gimelshein, Luca Antiga, Alban Desmaison, Andreas Kopf, Edward Yang, Zachary DeVito, Martin Raison, Alykhan Tejani, Sasank Chilamkurthy, Benoit Steiner, Lu Fang, Junjie Bai, and Soumith Chintala. Pytorch: An imperative style, high-performance deep learning library. In *Advances in Neural Information Processing Systems (NeurIPS)*. 2019. 16

## A Proofs.

We first start by defining Lipschitz continuity and the corresponding tightest Lipschitz constant.

**Proposition 1.** Consider a differentiable function  $g : \mathbb{R}^n \rightarrow \mathbb{R}$ . If  $\sup_x \|\nabla g(x)\|_* \leq L$  where  $\|\cdot\|_*$  has a dual norm  $\|z\| = \max_x z^\top x$  s.t.  $\|x\|_* \leq 1$ , then  $g$  is  $L$ -Lipschitz under norm  $\|\cdot\|_*$ , that is  $|g(x) - g(y)| \leq L\|x - y\|$ .

*Proof.* Consider some  $x, y \in \mathbb{R}^n$  and a parameterization in  $t$  as  $\gamma(t) = (1 - t)x + ty \quad \forall t \in [0, 1]$ . Note that  $\gamma(0) = x$  and  $\gamma(1) = y$ . By the fundamental Theorem of calculus we have:

$$\begin{aligned} |g(y) - g(x)| &= |g(\gamma(1)) - g(\gamma(0))| = \left| \int_0^1 \frac{dg(\gamma(t))}{dt} dt \right| = \left| \int_0^1 \nabla g^\top \nabla \gamma dt \right| \leq \int_0^1 |\nabla g^\top \nabla \gamma| dt \\ &\leq \int_0^1 \|\nabla g(x)\|_* \|\nabla \gamma(t)\| dt \leq L\|y - x\| \end{aligned}$$

□

To prove Theorem 1 and corollary 1, we note that any Lipschitz function is certifiable.

**Theorem 2.** Let  $f : \mathbb{R}^n \rightarrow \mathbb{R}$ ,  $f^i$  be  $L$ -Lipschitz continuous under norm  $\|\cdot\|_* \forall i \in \{1, \dots, K\}$ , and  $c_A = \arg \max_i f^i(x)$ . Then, we have  $\arg \max_i f^i(x + \delta) = c_A$  for all  $\delta$  satisfying:

$$\|\delta\| \leq \frac{1}{2L} \left( f^{c_A}(x) - \max_c f^{c \neq c_A}(x) \right).$$

*Proof.* Take  $c_B = \arg \max_c f^{c \neq c_A}(x)$ . Hence:

$$\begin{aligned} |f^{c_A}(x + \delta) - f^{c_A}(x)| &\leq L\|\delta\| \implies f^{c_A}(x + \delta) \geq f^{c_A}(x) - L\|\delta\| \\ |f^{c_B}(x + \delta) - f^{c_B}(x)| &\leq L\|\delta\| \implies f^{c_B}(x + \delta) \leq f^{c_B}(x) + L\|\delta\| \end{aligned}$$

By subtracting the inequalities and re-arranging terms, we have that as long as  $f^{c_A}(x) - L\|\delta\| > f^{c_B}(x) + L\|\delta\|$ , i.e. the bound in the Theorem, then  $f^{c_A}(x + \delta) > f^{c_B}(x + \delta)$ , completing the proof. □

Next, we deploy Theorem 2 to prove Theorem 1 and corollary 1. We first revisit the definition of a deformation smoothed classifier.

**Definition 1 (restatement).** Given a classifier  $f : \mathbb{R}^n \rightarrow \mathcal{P}(\mathcal{Y})$  and an interpolation function  $I_T : [0, 1]^n \times \mathbb{R}^{2|\Omega^Z|} \rightarrow [0, 1]^n$ , we define a deformation smoothed classifier as:

$$\hat{g}(x, p) = \mathbb{E}_{\epsilon \sim \mathcal{D}} [f(I_T(x, p + \epsilon))].$$

At first, following Theorem 2, we show that  $\hat{g}(x, p)$  is Lipschitz in  $p$ .

**Proposition 1.**  $\hat{g}(x, p) = \mathbb{E}_{\epsilon \sim \mathcal{U}[-\lambda, \lambda]} [f(I_T(x, p + \epsilon))]$  is  $1/2\lambda$ -Lipschitz in  $p$  under  $\|\cdot\|_\infty$  norm.

*Proof.* It suffices to show that  $\|\nabla_p \hat{g}(x, p)\|_\infty \leq 1/2\lambda$  to complete the proof. Without loss of generality, we analyze  $\partial \hat{g} / \partial p_1$ . Let  $\hat{p} = [p_2, \dots, p_n] \in \mathbb{R}^{n-1}$ , then:

$$\begin{aligned} \frac{\partial \hat{g}}{\partial p_1} &= \frac{1}{(2\lambda)^n} \frac{\partial}{\partial p_1} \int_{-\lambda}^{\lambda} \int_{-\lambda}^{\lambda} f(I_T(x, p_1 + \epsilon_1, \hat{p} + \hat{\epsilon})) d\epsilon_1 d^{n-1} \hat{\epsilon} \\ &= \frac{1}{(2\lambda)^n} \int_{-\lambda}^{\lambda} \frac{\partial}{\partial p_1} \int_{p_1 - \lambda}^{p_1 + \lambda} f(I_T(x, t, \hat{p} + \hat{\epsilon})) dt d^{n-1} \hat{\epsilon} \\ &= \frac{1}{(2\lambda)^n} \int_{-\lambda}^{\lambda} f(I_T(x, p_1 + \lambda, \hat{p} + \hat{\epsilon})) - f(I_T(x, p_1 - \lambda, \hat{p} + \hat{\epsilon})) dt d^{n-1} \hat{\epsilon} \end{aligned}$$

Thus,

$$\left| \frac{\partial \hat{g}}{\partial p_1} \right| \leq \frac{1}{(2\lambda)^n} \int_{-\lambda}^{\lambda} |f(I_T(x, p_1 + \lambda, \hat{p} + \hat{\epsilon})) - f(I_T(x, p_1 - \lambda, \hat{p} + \hat{\epsilon}))| dt d^{n-1} \hat{\epsilon} \leq \frac{1}{2\lambda}.$$

Where the second and last steps are accomplished through the change of variable  $t = p_1 + \epsilon_1$  and Leibniz rule. Similarly,  $|\partial \hat{g} / \partial p_i| \leq 1/2\lambda \forall i$ . This results in having  $\|\nabla_p \hat{g}(x)\|_\infty = \max_i |\partial \hat{g} / \partial p_i| \leq 1/2\lambda$ . □



At last, we show that the composite  $\Phi^{-1}(\hat{g}(x, p))$  is Lipschitz in  $p$  under  $\|\cdot\|_2$  norm.

following Theorem 2, we show that  $\hat{g}(x, p)$  is Lipschitz in  $p$ .

**Proposition 2.**  $\Phi^{-1}(\hat{g}(x, p)) = \Phi^{-1}(\mathbb{E}_{\epsilon \sim \mathcal{N}(0, \sigma^2 I)} [f(I_T(x, p + \epsilon))])$  is  $1/\sigma$ -Lipschitz in  $p$  under  $\|\cdot\|_2$  norm.

*Proof.* We want to show that  $\|\nabla \Phi^{-1}(\hat{g}(x, p))\|_2 \leq 1$ . Following the argument presented in [24], it suffices to show that, for any unit norm direction  $u$  and  $r = \hat{g}(x, p)$ , we have:

$$\sigma u^\top \nabla_p \hat{g}(x, p) \leq \frac{1}{\sqrt{2\pi}} \exp\left(-\frac{1}{2}(\Phi^{-1}(r))^2\right). \quad (3)$$

We start by noticing that:

$$\sigma u^\top \nabla_p \hat{g}(x, p) = \mathbb{E}_{v \sim \mathcal{N}(0, \sigma^2 I)} [f(I_T(x, p + v)) \frac{u^\top v}{\sigma}].$$

We now want to show that the function  $f : \mathbb{R}^n \rightarrow [0, 1]$ , note that  $f(I_T(x, p))$  is the function to be smoothed that maps to a probability simplex, which (i) satisfies  $\hat{g}(x, p) = \mathbb{E}_{v \sim \mathcal{N}(0, \sigma^2 I)} [f(I_T(x, p + v))]$  while (ii) maximizing  $\mathbb{E}_{v \sim \mathcal{N}(0, \sigma^2 I)} [f(I_T(x, p + v)) u^\top v / \sigma]$  is given by:

$$f^*(I_T(x, p + v)) = \mathbb{1} \left\{ \frac{u^\top v}{\sigma} \geq -\Phi^{-1}(r) \right\}.$$

To prove that  $f^*$  is the optimal solution we first show feasibility. (i): It is clear that  $f^* : \mathbb{R}^n \rightarrow [0, 1]$ , and note that (ii):

$$\mathbb{E}_{v \sim \mathcal{N}(0, \sigma^2 I)} \left[ \mathbb{1} \left\{ \frac{u^\top v}{\sigma} \geq -\Phi^{-1}(r) \right\} \right] = \mathbb{P}_{x \sim \mathcal{N}(0, 1)} (x \geq -\Phi^{-1}(r)) = 1 - \Phi(-\Phi^{-1}(r)) = r.$$

At last, we show that  $f^*$  attains the upper bound (ii):

$$\begin{aligned} \mathbb{E}_{v \sim \mathcal{N}(0, \sigma^2 I)} \left[ \mathbb{1} \left\{ \frac{u^\top v}{\sigma} \geq -\Phi^{-1}(r) \right\} \frac{u^\top v}{\sigma} \right] &= \mathbb{E}_{x \sim \mathcal{N}(0, 1)} [x \mathbb{1} \{x \geq -\Phi^{-1}(r)\}] \\ &= \frac{1}{\sqrt{2\pi}} \int_{-\Phi^{-1}(r)}^{\infty} x \exp\left(-\frac{1}{2}x^2\right) dx \\ &= \frac{1}{\sqrt{2\pi}} \exp\left(-\frac{1}{2}(\Phi^{-1}(r))^2\right), \end{aligned}$$

obtaining the bound from Equation (3), and thus completing the proof.  $\square$

**Theorem 1 (restatement).** Consider  $\hat{g}(x, p) = \mathbb{E}_{\epsilon \sim \mathcal{D}} [f(I_T(x, p + \epsilon))]$  where  $\hat{g}$  assigns the class  $c_A$  for an input  $x$ , i.e.  $c_A = \arg \max_c \hat{g}^c(x, p)$  with:

$$p_A = \hat{g}^{c_A}(x, p) \quad \text{and} \quad p_B = \max_{i \neq c_A} \hat{g}^i(x, p)$$

then  $\arg \max_c \hat{g}^c(x, p + \psi) = c_A$  for vector field perturbations satisfying:

$$\begin{aligned} \|\psi\|_1 &\leq \lambda (p_A - p_B) && \text{for } \mathcal{D} = \mathcal{U}[-\lambda, \lambda], \\ \|\psi\|_2 &\leq \frac{\sigma}{2} (\Phi^{-1}(p_A) - \Phi^{-1}(p_B)) && \text{for } \mathcal{D} = \mathcal{N}(0, \sigma^2 I), \end{aligned} \quad (4)$$

*Proof.* The proof follows immediately by substituting  $L$  and  $f(x)$  in Theorem 2 by  $L = 1/2\lambda$ ,  $\hat{g}(x, p)$  and  $L = 1/\sigma$ ,  $\Phi^{-1}(\hat{g}(x, p))$  for Uniform and Gaussian distributions, respectively. Due to the monotonicity of  $\Phi^{-1}$ ,  $\max_{i \neq c_A} \Phi^{-1}(\hat{g}^i(x, p)) = \Phi^{-1}(\max_{i \neq c_A} \hat{g}^i(x, p))$  completing the proof.  $\square$

**Corollary 1 (restatement).** Suppose that  $\tilde{g}$  assigns the class  $c_A$  for an input  $x$ , i.e.  $c_A = \arg \max_c \tilde{g}_\phi^c(x, p)$  with:

$$p_A = \tilde{g}_\phi^{c_A}(x, p) \quad \text{and} \quad p_B = \max_{i \neq c_A} \tilde{g}_\phi^i(x, p),$$

then  $\arg \max_c \tilde{g}_\phi^c(x, p) = c_A$  for all parametric domain perturbations satisfying:

$$\begin{aligned} \|\xi\|_1 &\leq \lambda (p_A - p_B) && \text{for } \mathcal{D} = \mathcal{U}[-\lambda, \lambda], \\ \|\xi\|_2 &\leq \frac{\sigma}{2} (\Phi^{-1}(p_A) - \Phi^{-1}(p_B)) && \text{for } \mathcal{D} = \mathcal{N}(0, \sigma^2 I). \end{aligned} \quad (5)$$

*Proof.* The proof is identical to the proof of Theorem 1 but with replacing  $\hat{g}$  with  $\tilde{g}$ , and  $p$  with  $\phi$ .  $\square$

## B Few Comments about the DCT Deformations

Discrete Cosine Transforms (DCT) expresses an input signal as a finite sum of cosines at different frequencies. We consider a single dimensional input  $T \in \mathbb{R}^N$  that denotes a transformation of a 1D dimensional signal of size  $N$  where the extension to the 2D follows immediately. The DCT of  $T$  is given as follows:  $\bar{T}_k = \sum_{n=0}^{N-1} a_n T_n \cos\left(\frac{\pi k}{N} \left(n + \frac{1}{2}\right)\right)$ , where  $k \in \{0, 1, \dots, N-1\}$ . Similarly to Discrete Fourier Transform, DCT is a linear operator, therefore it can be expressed in a matrix-vector multiplication as  $\bar{T} = \mathbf{C}T$  where  $\mathbf{C} \in \mathbb{R}^{N \times N}$  is the discrete cosine matrix such that  $\mathbf{C}_{i,j} = a_i \cos\left(\frac{\pi(i-1)}{2} \left((j-1) + \frac{1}{2}\right)\right)$ . Note that the number of basis of this transform is  $N$ , which is similar to the input dimension.

We consider certifying the truncated version of the DCT transformation where we have  $\tilde{N} \ll N$  basis, i.e.  $a_n = 0 \forall n \geq \tilde{N}$ . That is to say, a DCT certification of radius  $r$  as per Section 3.2 has the following form  $\|\xi\|_2 = \sqrt{\sum_i^{\tilde{N}} a_i^2} \leq r$ . The smooth classifier DEFORMRS-PAR is constructed by generating deformations using truncated DCT transformation and hence certifies the parameters of  $\tilde{N}$  basis. Throughout our experiments, we set  $\tilde{N} = 2$ ; we refer to  $\tilde{N}$  in the main manuscript as  $k \times k$  with  $k = 2$  representing the 2D DCT setting.

## C Code.

```
import math
import torch
import torch.nn as nn
import torch.nn.functional as F
from torch import meshgrid as mg

class DeformWrapper(nn.Module):
    def __init__(self, model, device, aug_method, sigma):
        super(DeformWrapper, self).__init__()
        self.base_classifier = model
        self.aug_method = aug_method
        self.sigma = sigma

    def _GenImageRotation(self, x):
        N, num_channels, rows, cols = x.shape # N is the batch size
        ang = (-2 * torch.rand((N, 1, 1)) + 1) * self.sigma
        # ang is sampled from Uniform between [-sigma, sigma]

        #Generating the vector field for rotation.
        X, Y = mg(torch.linspace(-1,1,rows), torch.linspace(-1,1,cols))
        X, Y = X.unsqueeze(0), Y.unsqueeze(0)
        Xv = X*torch.cos(ang)-Y*torch.sin(ang)-X
        Yv = X*torch.sin(ang)+Y*torch.cos(ang)-Y

        randomFlow = torch.stack((Yv,Xv), axis=3).to(self.device)
        grid = torch.stack((Y,X), axis=3).to(self.device)

        return F.grid_sample(x, grid+randomFlow)

    def _GenImageTranslation(self, x):
        N, _, rows, cols = x.shape #N is the batch size

        #Generating the vector field for translation.
        X, Y = mg(torch.linspace(-1,1,rows), torch.linspace(-1,1,cols))
        X, Y = X.unsqueeze(0), Y.unsqueeze(0)
        Xv = torch.randn((N, 1, 1))*self.sigma + 0*X
        Yv = torch.randn((N, 1, 1))*self.sigma + 0*Y

        randomFlow = torch.stack((Yv,Xv), axis=3).to(self.device)
        grid = torch.stack((Y,X), axis=3).to(self.device)
```

```

return F.grid_sample(x, grid+randomFlow)

def forward(self, x):
    elif self.aug_method == 'rotation':
        x = self._GenImageRotation(x)
    elif self.aug_method == 'translation':
        x = self._GenImageTranslation(x)
    else:
        raise Exception("Un identified augmentation method!")
    return self.base_classifier(x)

```

We will release the full code that reproduces all of our results after the reviewing period. Nevertheless, we attached the main component of our code in *deform-wrapper.py* that is written in PyTorch [36]. This class takes a classifier and an augmentation method along with its smoothing parameter. The forward pass of this class is a forward of a deformed sample to the base classifier. We provide, nonetheless, a snippet of it here in the appendix that corresponds to translation and rotation deformations. During certification, we use the approach of Cohen [8] in their official released code in <https://github.com/locuslab/smoothing/tree/master/code>.

## D Limitations, Broader Impact, and Compute Power.

**Limitations.** The main limitation of this work, and any certification work, is the running time to compute the prediction of the classifier, and the certified radius around a given input point. However and since we deployed randomized smoothing, this affordable extra computation comes with the benefit of providing a network that is not only accurate, but certifiable robust against a variety of input deformations.

**Broader Impact.** Deep Neural Networks (DNNs) have achieved state-of-the-art results in a variety of computer vision tasks. However, this impressive performance was shown to be brittle against imperceptible input variations. These variations could be not only input perturbations (varying pixel intensities) but also geometric transformations (*e.g.* rotating the input image). Since these variations are likely to happen in real world scenarios, as the camera might experience some accidental movements, the deployment of DNNs in safety-critical applications (*e.g.* self driving cars) is limited. This work takes a step into solving this issue by building classifiers that are certifiably robust against a variety of input deformations and hence increase the reliability of DNNs.

**Compute Power.** In all of our training experiments, we used a single NVIDIA 1080-TI for CIFAR10 and MNIST experiments while we used 2 NVIDIA V100 to fine tune ImageNet models. For the certification experiments, we use a single gpu per experiments ( NVIDIA 1080-TI for CIFAR10 and MNIST and NVIDIA V100 for ImageNet ).

## E Visualizations.

We provide more samples that are within the certifiable radius for affine, DCT, and VF deformations. For affine, we show in Figure 6 2 examples from CIFAR10 (left) and ImageNet (right). For DCT deformation, we show in Figure 7 4 examples from both MNIST (right) and CIFAR19 (left). Note that all samples are classified correctly, as the norm of their DCT parameters is less than the certified radius. Moreover, it is to observe that DCT deformations provide semantically meaningful deformations presented as ripples and stretches. Last, we provide 8 examples of certifiable full VF deformations in Figure 8. Note that since the certified norm is small, some of these deformations are imperceptible (specially on MNIST). We also noticed that some samples in CIFAR10 obtained large certified radius, hence could resist perceptible deformations as shown in the last row. We believe that this is due to the fact that rgb images are easier to discriminate not only based on texture, but also based on colors.

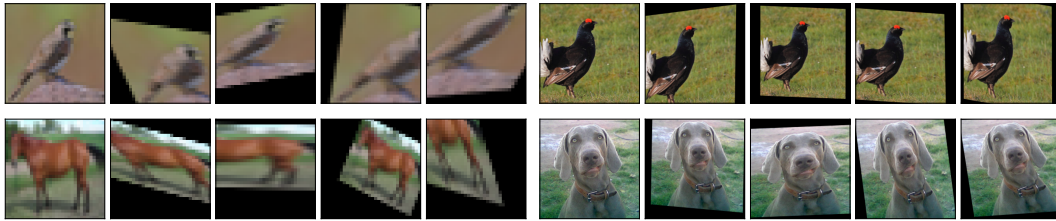


Figure 6: **Certified examples against affine deformations.** The Figure shows 4 ImageNet images and several examples of affine deformations that are certifiable, i.e. DEFORMRS-PAR produces a correct prediction under all the deformed examples.

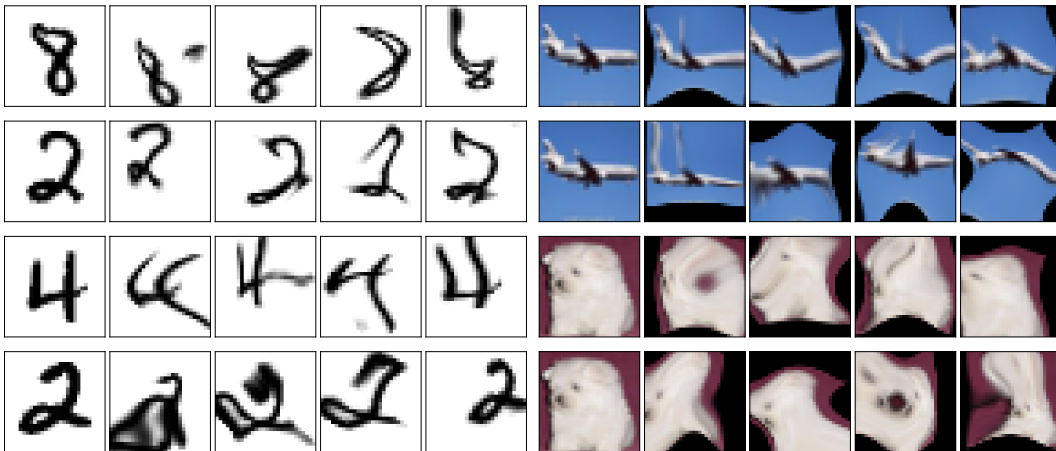


Figure 7: **Certified examples against DCT deformations.** The Figure shows 2 MNIST and 2 CIFAR10 images and several examples of DCT deformations that are certifiable, i.e. DEFORMRS-PAR produces a correct prediction under all the deformed examples.



Figure 8: **Certified examples against vector field deformations.** The Figure shows 2 MNIST and 2 CIFAR10 images along with several vector field deformed images that are certifiable, i.e. DEFORMRS-PAR produces a correct prediction under all the deformed examples.

Table 3: **Rotation Ablations.** The tables show the certified accuracy on MNIST, CIFAR10 and ImageNet for DEFORMRS-PAR while varying the certified rotation radius, *i.e.*  $|\theta| \leq r$ , for different networks trained with different  $\lambda$ .

MNIST	0°	10°	30°	45°	60°	90°	120°	135°	150°	180°	ACR°
$\lambda = 1\pi/10$	98.81	98.06	0.0	0.0	0.0	0.0	0.0	0.0	0.0	0.0	17.64
$\lambda = 2\pi/10$	98.86	98.37	96.49	0.0	0.0	0.0	0.0	0.0	0.0	0.0	35.10
$\lambda = 3\pi/10$	98.28	97.91	96.85	95.14	0.0	0.0	0.0	0.0	0.0	0.0	52.14
$\lambda = 4\pi/10$	96.59	95.92	94.33	92.61	90.06	0.0	0.0	0.0	0.0	0.0	67.15
$\lambda = 5\pi/10$	97.36	97.09	96.28	95.48	94.05	0.0	0.0	0.0	0.0	0.0	85.04
$\lambda = 6\pi/10$	95.55	95.21	94.09	92.95	91.75	87.70	0.0	0.0	0.0	0.0	98.48
$\lambda = \pi$	94.55	94.37	93.85	93.18	92.54	91.31	89.62	88.66	87.52	0.0	163.12
CIFAR10	0°	10°	30°	45°	60°	90°	120°	135°	150°	180°	ACR°
$\lambda = 3\pi/10$	93.07	91.82	87.77	82.68	0.0	0.0	0.0	0.0	0.0	0.0	47.17
$\lambda = 4\pi/10$	92.56	91.46	88.75	85.61	80.66	0.0	0.0	0.0	0.0	0.0	62.17
$\lambda = 5\pi/10$	91.49	90.67	88.28	86.24	83.20	0.0	0.0	0.0	0.0	0.0	76.06
$\lambda = 6\pi/10$	91.21	90.55	88.63	87.12	85.03	77.84	0.0	0.0	0.0	0.0	90.70
$\lambda = 7\pi/10$	90.64	90.13	88.21	86.87	85.18	80.93	70.83	0.0	0.0	0.0	117.78
$\lambda = 8\pi/10$	88.88	88.30	87.18	86.00	84.56	81.47	76.14	70.37	0.0	0.0	105.05
$\lambda = 9\pi/10$	88.11	87.62	86.66	85.81	84.76	82.23	78.97	76.13	71.95	0.0	132.3
$\lambda = \pi$	43.28	40.04	33.79	29.31	25.59	18.57	12.72	10.51	8.10	0.0	36.50
ImageNet	0°	10°	30°	45°	60°	90°	120°	135°	150°	180°	ACR°
$\lambda = 5\pi/10$	40.60	39.40	36.80	35.20	34.20	29.00	24.20	21.60	19.80	17.00	73.12
$\lambda = 6\pi/10$	40.00	39.00	34.80	32.60	30.00	23.00	0.0	0.0	0.0	0.0	32.73
$\lambda = 7\pi/10$	38.40	37.20	34.20	32.40	30.40	26.00	15.80	0.0	0.0	0.0	36.36
$\lambda = 8\pi/10$	36.80	36.20	33.80	32.40	30.80	27.60	21.40	16.40	0.0	0.0	40.52
$\lambda = 9\pi/10$	36.80	36.20	34.00	32.40	31.40	28.40	23.60	20.20	17.00	0.0	45.08

## F Ablations.

We provide here an ablation study to the effect of the parameters of the smoothing distribution to the performance of our smooth classifier. Not that as expected, the larger the smoothing parameters (*i.e.*  $\lambda$  and  $\sigma$ ), the certified classifier has smaller certified accuracy with small radii, but more samples are certified with larger radii. This trade off is demonstrated in all reported tables.



Table 4: **Scaling Ablations.** The tables show the certified accuracy on MNIST, CIFAR10 and ImageNet for DEFORMRS-PAR while varying the certified scaling radius, *i.e.*  $|\alpha - 1| \leq r$ , for different networks trained with different  $\lambda$ .

MNIST	0%	10%	20%	30%	40%	50%	60%	70%	80%	90%	ACR
$\lambda = 10\%$	97.94	0.0	0.0	0.0	0.0	0.0	0.0	0.0	0.0	0.0	0.10
$\lambda = 20\%$	97.98	96.76	0.0	0.0	0.0	0.0	0.0	0.0	0.0	0.0	0.19
$\lambda = 30\%$	97.96	97.35	95.85	0.0	0.0	0.0	0.0	0.0	0.0	0.0	0.29
$\lambda = 40\%$	92.84	91.63	89.83	87.64	0.0	0.0	0.0	0.0	0.0	0.0	0.36
$\lambda = 50\%$	99.00	98.88	98.70	98.36	97.46	0.0	0.0	0.0	0.0	0.0	0.49
$\lambda = 60\%$	97.51	97.04	96.07	95.16	93.48	89.87	0.0	0.0	0.0	0.0	0.56
$\lambda = 70\%$	98.79	98.70	98.41	97.96	97.13	95.65	91.33	0.0	0.0	0.0	0.67

CIFAR10	0%	10%	20%	30%	40%	50%	60%	70%	80%	90%	ACR
$\lambda = 10\%$	93.93	0.0	0.0	0.0	0.0	0.0	0.0	0.0	0.0	0.0	0.09
$\lambda = 20\%$	93.88	91.57	0.0	0.0	0.0	0.0	0.0	0.0	0.0	0.0	0.18
$\lambda = 30\%$	94.10	92.48	89.48	0.0	0.0	0.0	0.0	0.0	0.0	0.0	0.27
$\lambda = 40\%$	93.72	92.38	90.33	86.76	0.0	0.0	0.0	0.0	0.0	0.0	0.36
$\lambda = 50\%$	93.34	92.10	90.31	87.70	83.29	0.0	0.0	0.0	0.0	0.0	0.44
$\lambda = 60\%$	93.53	92.18	90.53	88.32	84.87	78.77	0.0	0.0	0.0	0.0	0.52
$\lambda = 70\%$	92.73	91.76	90.25	88.24	85.00	80.30	71.44	0.0	0.0	0.0	0.58

ImageNet	0%	10%	20%	30%	40%	50%	60%	70%	80%	90%	ACR
$\lambda = 10\%$	51.00	0.0	0.0	0.0	0.0	0.0	0.0	0.0	0.0	0.0	0.05
$\lambda = 20\%$	50.60	44.40	0.0	0.0	0.0	0.0	0.0	0.0	0.0	0.0	0.09
$\lambda = 30\%$	49.60	45.60	40.00	0.0	0.0	0.0	0.0	0.0	0.0	0.0	0.13
$\lambda = 40\%$	48.20	45.20	40.80	34.00	0.0	0.0	0.0	0.0	0.0	0.0	0.16
$\lambda = 50\%$	46.80	42.80	38.80	33.60	28.00	0.0	0.0	0.0	0.0	0.0	0.18
$\lambda = 60\%$	46.00	43.00	40.00	33.40	27.00	20.00	0.0	0.0	0.0	0.0	0.19
$\lambda = 70\%$	45.00	42.20	39.00	32.80	25.40	20.60	11.20	0.0	0.0	0.0	0.20

Table 5: **Translation Ablations.** The tables show the certified accuracy on MNIST, CIFAR10 and ImageNet for DEFORMRS-PAR while varying the certified translation radius, *i.e.*  $\sqrt{t_u^2 + t_v^2} \leq r$ , for different networks trained with different  $\sigma$ .

MNIST	2	4	6	8	10	12	14	16	18	20	ACR
$\sigma = 0.1$	98.50	97.73	0.0	0.0	0.0	0.0	0.0	0.0	0.0	0.0	5.23
$\sigma = 0.2$	98.88	98.57	97.86	95.01	73.95	0.0	0.0	0.0	0.0	0.0	10.01
$\sigma = 0.3$	98.94	98.71	98.22	96.50	89.66	69.20	31.26	0.0	0.0	0.0	12.74
$\sigma = 0.4$	99.05	98.76	98.14	96.37	89.32	72.99	38.37	7.66	0.15	0.0	13.04
$\sigma = 0.5$	99.06	98.68	97.82	94.70	84.84	62.77	29.20	5.48	0.19	0.0	12.48

CIFAR10	2	4	6	8	10	13	16	19	22	25	ACR
$\sigma = 0.1$	89.88	83.75	73.04	0.0	0.0	0.0	0.0	0.0	0.0	0.0	5.25
$\sigma = 0.2$	91.90	88.95	84.61	78.67	69.07	0.0	0.0	0.0	0.0	0.0	9.81
$\sigma = 0.3$	92.48	90.35	87.21	82.44	75.79	59.52	32.63	0.0	0.0	0.0	12.71
$\sigma = 0.4$	92.55	90.46	87.65	83.60	77.94	64.79	43.95	22.24	4.28	0.0	14.03
$\sigma = 0.5$	92.20	90.37	87.19	82.80	77.79	64.59	45.99	26.59	9.98	1.52	14.39

ImageNet	2	4	6	8	10	13	16	19	22	25	ACR
$\sigma = 0.02$	46.80	42.20	35.00	31.80	0.0	0.0	0.0	0.0	0.0	0.0	3.48
$\sigma = 0.03$	47.80	44.00	40.20	35.60	32.80	0.0	0.0	0.0	0.0	0.0	5.02
$\sigma = 0.04$	49.20	45.40	42.20	38.80	35.80	31.80	27.80	0.0	0.0	0.0	6.57
$\sigma = 0.05$	48.60	46.00	43.20	41.00	38.20	34.80	31.80	28.40	0.0	0.0	8.10
$\sigma = 0.06$	49.20	47.60	45.20	43.20	40.40	36.80	34.80	31.40	28.20	24.40	9.70

Table 6: **Affine Ablations.** The tables show the certified accuracy on MNIST, CIFAR10 and ImageNet for DEFORMRS-PAR while varying the certified affine radius, *i.e.*  $\sqrt{a^2 + b^2 + c^2 + d^2 + e^2 + f^2} \leq r$ , for different networks trained with different  $\sigma$ .

MNIST	0.1	0.2	0.3	0.4	0.5	0.6	0.7	0.8	0.9	1.0	ACR
$\sigma = 0.1$	98.64	97.50	94.67	0.0	0.0	0.0	0.0	0.0	0.0	0.0	0.37
$\sigma = 0.2$	99.08	98.49	97.31	93.79	80.38	37.58	7.55	0.0	0.0	0.0	0.56
$\sigma = 0.3$	98.70	97.85	96.15	91.19	76.13	36.39	6.78	0.74	0.0	0.0	0.55
$\sigma = 0.4$	98.19	96.88	93.50	82.34	51.44	13.45	0.77	0.0	0.0	0.0	0.49
CIFAR10	0.1	0.2	0.3	0.4	0.5	0.6	0.7	0.8	0.9	1.0	ACR
$\sigma = 0.1$	89.31	81.23	65.92	0.0	0.0	0.0	0.0	0.0	0.0	0.0	0.30
$\sigma = 0.2$	90.51	85.50	77.11	64.68	46.46	22.08	2.93	0.0	0.0	0.0	0.44
$\sigma = 0.3$	88.09	82.81	75.66	65.33	50.84	32.98	15.72	4.59	0.57	0.01	0.46
$\sigma = 0.4$	83.20	77.60	69.53	58.77	45.94	31.07	17.97	8.17	2.87	0.90	0.44
$\sigma = 0.5$	75.40	69.06	61.15	50.95	39.22	27.88	18.06	9.71	4.83	2.00	0.40
ImageNet	0.02	0.04	0.06	0.08	0.10	0.12	0.14	0.16	0.18	0.20	ACR
$\sigma = 0.03$	48.00	43.60	37.20	30.40	26.20	0.0	0.0	0.0	0.0	0.0	0.04
$\sigma = 0.04$	49.00	45.20	40.60	35.20	29.60	27.80	24.00	0.0	0.0	0.0	0.06
$\sigma = 0.05$	48.60	46.20	42.80	38.40	33.60	30.20	27.40	24.60	19.80	0.0	0.07
$\sigma = 0.06$	49.00	45.80	44.20	40.60	36.60	32.80	29.20	27.80	24.00	21.20	0.08

Table 7: **DCT Ablations.** The tables show the certified accuracy on MNIST and CIFAR10 for DEFORMRS-PAR while varying the certified DCT radius, *i.e.*  $\|\xi\|_2 \leq r$ , for different networks trained with different  $\sigma$ .

MNIST	0.1	0.2	0.3	0.4	0.5	0.6	0.7	0.8	0.9	1.0	ACR
$\sigma = 0.1$	97.58	91.66	61.55	0.0	0.0	0.0	0.0	0.0	0.0	0.0	0.30
$\sigma = 0.2$	96.20	89.89	76.07	49.21	18.83	0.61	0.0	0.0	0.0	0.0	0.38
$\sigma = 0.3$	92.40	82.18	64.55	44.34	22.52	6.73	0.63	0.0	0.0	0.0	0.36
$\sigma = 0.4$	86.93	72.50	51.05	31.33	15.07	6.08	1.99	0.12	0.0	0.0	0.31
$\sigma = 0.5$	69.10	54.58	37.08	20.86	12.05	6.36	3.68	1.06	0.04	0.0	0.25
$\sigma = 0.6$	49.16	35.42	21.58	12.23	7.31	5.09	2.97	0.91	0.03	0.0	0.17
CIFAR10	0.1	0.2	0.3	0.4	0.5	0.6	0.7	0.8	0.9	1.0	ACR
$\sigma = 0.1$	83.23	66.45	39.66	0.0	0.0	0.0	0.0	0.0	0.0	0.0	0.24
$\sigma = 0.2$	79.42	69.47	56.33	40.48	25.17	12.21	3.03	0.0	0.0	0.0	0.33
$\sigma = 0.3$	74.47	66.86	57.66	47.74	37.21	27.14	17.73	10.15	4.48	1.15	0.39
$\sigma = 0.4$	69.92	63.95	56.94	49.68	42.21	34.36	26.43	19.20	12.64	7.24	0.43
$\sigma = 0.5$	66.75	61.49	56.07	50.22	44.11	37.86	31.08	24.68	18.53	13.03	0.46
$\sigma = 0.6$	62.78	58.25	53.78	48.99	43.72	38.35	32.76	27.06	21.62	16.33	0.47

Table 8: **Vector Field Ablations.** The tables show the certified accuracy on MNIST and CIFAR10 for DEFORMRS-PAR while varying the certified vector field radius, *i.e.*  $\|\psi\|_2 \leq r$ , for different networks trained with different  $\sigma$ .

MNIST	1.0	2.0	3.0	4.0	5.0	6.0	7.0	8.0	9.0	10	ACR
$\sigma = 0.1$	95.41	90.18	79.55	60.31	31.02	0.0	0.0	0.0	0.0	0.0	4.01
$\sigma = 0.2$	79.26	69.04	55.2	40.37	26.22	15.39	7.99	3.90	1.45	0.28	3.42
$\sigma = 0.3$	23.04	16.96	12.29	9.00	6.79	5.40	4.21	3.26	2.49	1.96	1.05
$\sigma = 0.4$	15.75	11.74	8.52	5.80	4.12	2.93	2.13	1.40	0.87	0.47	0.64
$\sigma = 0.5$	12.96	10.54	8.47	6.79	5.27	4.02	3.03	2.38	1.91	1.48	0.70
$\sigma = 0.6$	13.02	11.12	9.51	8.05	6.70	5.65	4.79	3.93	3.16	2.63	0.84
$\sigma = 0.7$	11.23	9.96	8.71	7.91	6.86	6.17	5.56	4.79	4.19	3.70	0.92
$\sigma = 0.8$	10.85	9.93	9.05	8.42	7.81	7.24	6.62	5.90	5.39	4.92	1.09
$\sigma = 0.9$	11.45	10.46	9.62	8.90	8.20	7.50	6.84	6.30	5.74	5.16	1.26
CIFAR10	1.0	2.0	3.0	4.0	5.0	6.0	7.0	8.0	9.0	10	ACR
$\sigma = 0.1$	75.83	69.48	63.23	55.67	46.90	32.10	0.0	0.0	0.0	0.0	3.73
$\sigma = 0.2$	66.77	63.01	59.40	55.38	51.13	46.98	42.63	37.79	33.47	29.29	5.58
$\sigma = 0.3$	61.84	59.09	56.13	53.03	50.02	47.14	44.50	41.56	38.68	35.55	6.98
$\sigma = 0.4$	58.56	56.41	54.12	51.67	49.59	47.27	44.98	42.84	40.64	38.36	8.28
$\sigma = 0.5$	56.18	54.45	52.36	50.78	49.02	47.23	45.36	43.61	42.11	40.58	9.67
$\sigma = 0.6$	54.39	53.07	51.59	50.24	48.85	47.24	45.59	44.06	42.40	40.96	10.96
$\sigma = 0.7$	53.37	52.24	51.00	49.73	48.39	47.29	46.07	44.83	43.73	42.35	12.47
$\sigma = 0.8$	51.48	50.42	49.29	48.24	47.09	46.01	44.96	43.88	42.83	41.74	13.57
$\sigma = 0.9$	50.69	49.69	48.72	47.76	46.80	45.70	44.81	43.66	42.83	41.83	14.61